Experimental Evaluation of Noise Parameters in Gunn and Avalanche Oscillators

MOTOHARU OHTOMO

Abstract—Equations are presented that express noise-to-carrier ratio and rms frequency deviation of a negative-resistance oscillator with a multiple-resonant circuit in terms of effective available noise power densities of both $1/f$ and white-noise sources, an effective saturation factor, and an appropriate Q_L of the oscillator. Experimental evaluation of the noise parameters in Gunn and avalanche oscillators by use of these equations is described.

AM and FM noise measurements have been made on *X*-band Gunn oscillators and Si and GaAs avalanche oscillators for frequency off carriers extending from 1 kHz to 10 MHz. Both $1/f$ and white noise have been observed in these oscillators.

The validity of the above equations has been verified for Gunn oscillators from the dependence of the noise spectra on Q_L. For Gunn oscillators and Si and GaAs avalanche oscillators, the effective noise-temperature ratio for white noise, N/kT_0, has been found to be 23~29, 41~51, and 38~44 dB, and the effective saturation factor to be 2~2.9, 0.5~2.4, and 2, respectively. An increase of N/kT_0 with the RF voltage across the diode has been observed in Si avalanche oscillators. Parameters for $1/f$ noise have also been evaluated approximately.

I. Introduction

GUNN AND AVALANCHE oscillators are now becoming useful microwave sources in practical applications such as local oscillators and low-power transmitters. Noise inherent in these oscillators is an important factor for these applications, and noise spectra of these devices have been measured and investigated by several workers [1]–[5]. Edson [6] and Mullen [7] individually developed the theory of noise in oscillators and obtained essentially the same results for output power spectra. Reformulation of the theory has been undertaken by Kurokawa [8]. To simplify the treatments, however, these theories have been developed under the conditions that 1) the oscillator consists of a single-tuned *LCR* circuit, 2) nonlinear characteristics of the negative resistance or conductance of the device are considered, while those of the reactance or susceptance are neglected, and 3) only a white-noise source is considered, except in [8]. Using Edson's theory, Josenhans [1] has given the expressions for noise-to-carrier ratio and rms frequency deviations, which are generally used to specify oscillator noise. Here they are called "Edson's equations" for brevity. The effective noise temperature and the saturation factor included in the equations are important device parameters governing noise characteristics of oscillators. Experimental evaluation of these parameters will be of great use in designing an oscillator in which noise is a great concern. The equations, however, are restricted by the above conditions, which are not necessarily obeyed by actual oscillators. This may be one of the reasons why there have been few papers published that dealt with the experimental evaluation of these parameters [1]. Recently, generalized theories of noise in oscillators have been developed by Kurokawa [9] and Okabe and Okamura [10] to remove these limitations. Their results are given in elegant but such general expressions that one might at first sight find some difficulties in applying them to the interpretation of measured noise spectra. The interpretation, however, will be facilitated if a relation between an oscillator Q and the frequency derivative of a circuit impedance is introduced.

The purpose of this paper is to present generalized Edson's equations in terms of the suitably defined parameters, to report on the AM and FM noise measurements of *X*-band Gunn and avalanche diode (Si and GaAs) oscillators, and to describe the evaluation of the noise parameters in the generalized Edson's equations. In Section II, definition of noise is first described, and the generalized Edson's equations for an oscillator with a multiple-resonant circuit are derived from Kurokawa's theory [9] by defining an appropriate Q_L of the oscillator and available noise power densities of $1/f$, as well as white-noise sources and an effective saturation factor. In Section III, the method of noise measurement is described in detail so as to show that accurate measurements can be performed with careful calibrations over a wide range of frequency off carrier from 1 kHz to 10 MHz. In Section IV, the results of the measurements on Gunn and avalanche oscillators and the evaluation of their noise parameters are given.

II. Specification of Noise in Oscillators

A. Definition of Noise

The output waveform of an oscillator is usually expressed by

$$U(t) = A_0\{1 + a(t)\} \cos \{\omega_0 t + \phi(t)\} \qquad (1)$$

where $U(t)$ represents a voltage or current, A_0 and ω_0 are the peak amplitude and the angular frequency of the carrier, respectively, and $a(t)$ and $\phi(t)$ are real functions of time varying slowly as compared to $\cos \omega_0 t$. Noise

Manuscript received July 14, 1971; revised September 7, 1971.
The author is with the Toshiba Research and Development Center, Tokyo Shibaura Electric Company, Ltd., Kawasaki, Japan.

sidebands arise from AM and PM (or FM) modulation of the carrier by real random variables $a(t)$ and $\phi(t)$ [or $\dot{\phi}(t)$], respectively.

When $a(t)$ and $\phi(t)$ are stationary random variables, they have auto- and crosscorrelation functions $R_a(\tau)$, $R_\phi(\tau)$, and $R_{a\phi}(\tau)$ from the inverse Fourier transform of which power spectral densities $S_a(f)$ and $S_\phi(f)$ and cross-spectral density $S_{a\phi}(f)$ are obtained [11]. The autocorrelation function of $U(t)$ is given by

$$\begin{aligned} R_U(\tau) &= A_0^2 \overline{[1+a(t)][1+a(t+\tau)]\cos[\omega_0 t+\phi(t)]\cos[\omega_0 t+\omega_0\tau+\phi(t+\tau)]} \\ &= \tfrac{1}{2} A_0^2 \overline{[1+a(t)a(t+\tau)+a(t)+a(t+\tau)][\cos\omega_0\tau\cos\{\phi(t+\tau)-\phi(t)\}-\sin\omega_0\tau\sin\{\phi(t+\tau)-\phi(t)\}]}. \end{aligned} \quad (2)$$

If $|a(t)| \ll 1$, $|\phi(t)| \ll 1$, and $|\phi(t+\tau)-\phi(t)| \ll 1$ are satisfied, the above equation is approximately calculated to be

$$\begin{aligned} R_U(\tau) = \frac{1}{4} A_0^2 \int_{-\infty}^{\infty} & [\{1-R_\phi(0)\}\{\delta(f-f_0)+\delta(f+f_0)\} \\ & + \{S_a(f-f_0)+S_a(f+f_0)\} \\ & + \{S_\phi(f-f_0)+S_\phi(f+f_0)\} \\ & + \{C_{a\phi}(f-f_0)-C_{a\phi}(f+f_0)\}]e^{j\omega\tau}\,df \end{aligned} \quad (3)$$

where the terms to the second order of $a(t)$ and $\phi(t)$ are retained, $\delta(f)$ is the delta function, and $C_{a\phi}(f)$ is defined by

$$C_{a\phi}(f) = -2\,\mathrm{Im}\{S_{a\phi}(f)\} \quad (4)$$

where Im denotes "imaginary part of." If we consider only the high-frequency components of $\phi(t)$ or make measurements in a time much shorter than the period of coherence τ_c [6], $\overline{\phi(t)^2}$ can be considered to be much less than one. Then the first term in the integrand of (3) represents a carrier spectrum, and the second, third, and fourth terms correspond to AM, PM, and AM–PM correlation noise spectra, respectively.

Since $S_a(f)$, $S_\phi(f)$, and $S_{a\phi}(f)$ are considered to be dominant around $f \ll f_0$ by the assumption that $a(t)$ and $\phi(t)$ are slowly varying functions of time as compared with $\cos\omega_0 t$, the inequalities $S_a(f-f_0) \gg S_a(f+f_0)$, $S_\phi(f-f_0) \gg S_\phi(f+f_0)$, and $C_{a\phi}(f-f_0) \gg C_{a\phi}(f+f_0)$ will generally hold. The [double-sideband (DSB) noise power contained in a bandwidth B around frequency $\pm f_m$ away from carrier] to (carrier power) ratio is then given by

$$(N/C)_{\mathrm{AM,DSB}} = 2S_a(f_m)B \quad (5)$$

$$(N/C)_{\mathrm{PM,DSB}} = 2S_\phi(f_m)B \quad (6)$$

for $f_m \gg 1/\tau_c$. If AM–PM correlation exists, noise sidebands become asymmetrical about the carrier, since $C_{a\phi}(f_m) = -C_{a\phi}(-f_m)$. The correlation terms cancel out, however, if we take the sum of both sidebands.

The rms frequency deviation in a bandwidth B is given by [12]

$$\Delta f_{\mathrm{rms}} = \frac{1}{2\pi}\sqrt{2S_{\dot{\phi}}(f_m)B} = \sqrt{2f_m^2 S_\phi(f_m)B}. \quad (7)$$

From (6) and (7), one obtains the relation

$$(N/C)_{\mathrm{PM,DSB}} = \Delta f_{\mathrm{rms}}^2/f_m^2. \quad (8)$$

B. Generalized Edson's Equations

An oscillator is generally represented by the circuit shown in Fig. 1(a) [9]. The active device represented by $-\overline{R}+j\overline{X}$ and the load R_L are coupled through a multiple-resonant reciprocal circuit. Looking from the active device, the circuit can be equivalently expressed, as shown in Fig. 1(b), where $e(t)$ represents equivalent noise voltages or injected signal voltage. The similar representation of an oscillator can also be obtained in terms of admittances. Both representations are dual to each other.

Let us now neglect the frequency dependence of $\overline{R}$ and $\overline{X}$, which is generally justifiable over the frequency of interest. According to Kurokawa [9], the equations governing the amplitude and phase fluctuations $a(t)$ and $\phi(t)$ are represented by

$$\alpha a(t) + |Z'(\omega_0)|^2 \frac{da(t)}{dt} = \frac{X'(\omega_0)}{A_0}[n_1(t)+n_R(t)] + \frac{R'(\omega_0)}{A_0}[n_2(t)+n_X(t)] \quad (9)$$

$$\beta a(t) + |Z'(\omega_0)|^2 \frac{d\phi(t)}{dt} = \frac{R'(\omega_0)}{A_0}[n_1(t)+n_R(t)] - \frac{X'(\omega_0)}{A_0}[n_2(t)+n_X(t)] \quad (10)$$

where $n_1(t)$ and $n_2(t)$ are the cosine and sine voltage components of the white-noise source (RF noise source), respectively, and $n_R(t)$ and $n_X(t)$ are the equivalent voltage components of $1/f$ noise. Although $n_R(t)$ and $n_X(t)$ have not been included in Kurokawa's paper [9], they can be introduced as above by defining $n_R(t) \equiv -A_0\Delta R$ and $n_X(t) \equiv A_0\Delta X$, where ΔR and ΔX are the fluctuating parts of $R(\omega)-\overline{R}$ and $X(\omega)+\overline{X}$, respectively, in equations (8) and (9) of [9]. Such procedures of introducing $1/f$ noise[1] have been described earlier by Kurokawa [8]. The coefficients α and β are defined by

$$\begin{aligned} \alpha &= sR_0X'(\omega_0) - rR_0R'(\omega_0) \\ &= R_0|Z'(\omega_0)|\sqrt{s^2+r^2}\sin(\Theta-\theta) \end{aligned} \quad (11)$$

$$\begin{aligned} \beta &= sR_0R'(\omega_0) + rR_0X'(\omega_0) \\ &= R_0|Z'(\omega_0)|\sqrt{s^2+r^2}\cos(\Theta-\theta) \end{aligned} \quad (12)$$

[1] The term $1/f$ noise is employed throughout this paper, though the term modulation noise may be more adequate, since fluctuations ΔR and ΔX may have various origins and may not always have $1/f$ dependence [3].

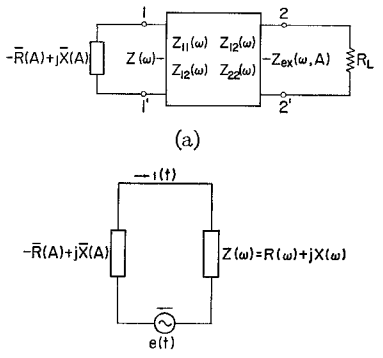

Fig. 1. (a) Schematic diagram for an oscillator. (b) Its equivalent circuit.

where

$$R_0 = \bar{R}(A_0)$$
$$Z'(\omega_0) = R'(\omega_0) + jX'(\omega_0) = |Z'(\omega_0)|e^{j\Theta}$$
$$sR_0 = -A_0\frac{d\bar{R}}{dA}$$
$$rR_0 = A_0\frac{d\bar{X}}{dA}$$
$$s + jr = \sqrt{s^2+r^2}\,e^{j\vartheta}.$$

For stable operation of the oscillator, $\sin(\Theta-\theta)>0$ is required [9].

From the differential equations (9) and (10), the power spectral densities of $a(t)$ and $\phi(t)$ are calculated to be

$$S_a(f) = \frac{1}{A_0^2}\frac{2|Z'|^2|e|^2 + X'^2S_{n_R}(f) + R'^2S_{n_X}(f) + 2X'R'\,\mathrm{Re}\{S_{n_Rn_X}(f)\}}{|Z'|^4\omega^2+\alpha^2} \tag{13}$$

$$S_\phi(f) = \frac{1}{\omega^2|Z'|^4A_0^2}\left[2|Z'|^2|e|^2 + R'^2S_{n_R}(f) + X'^2S_{n_X}(f) - 2X'R'\,\mathrm{Re}\{S_{n_Rn_X}(f)\} - 2\frac{\beta}{\omega}\mathrm{Im}\{S_{n_Rn_X}(f)\} + \beta^2A_0^2S_a(f)\right]. \tag{14}$$

where $|Z'(\omega_0)|$, $X'(\omega_0)$, and $R'(\omega_0)$ are abbreviated as $|Z'|$, X', and R', respectively, $S_{n_1}(f)=S_{n_2}(f)\equiv 2|e|^2$, and correlations between $n_1(t)$, $n_2(t)$, and $n_R(t)$ or $n_X(t)$ are assumed to be absent. Cross-spectral densities $S_{a\phi}$, $S_{a\phi}$, etc., can also be obtained and $C_{a\phi}(f)$, defined by (4), is calculated to be

$$C_{a\phi}(f) = \frac{2}{\omega^2|Z'|^4A_0^2}\left[-\omega\beta|Z'|^2A_0^2S_a(f) + |Z'|^2\,\mathrm{Im}\{S_{n_Rn_X}(f)\}\right].$$

As shown in the Appendix, Q_{ex} of an oscillator measured from injection-locking or frequency-pulling experiments is represented by

$$Q_{ex} = Q_{ex,c}\sin(\Theta-\theta) = \frac{\omega_0|Z_{ex}'(\omega_0)|}{2R_L}\sin(\Theta-\theta) \tag{15}$$

where $Z_{ex}'(\omega_0)\equiv[\partial Z_{ex}(\omega,A)/\partial\omega]_{\omega=\omega_0,A=A_0}$ and $Q_{ex,c}=\omega_0|Z_{ex}'(\omega_0)|/2R_L$ is termed the "Q_{ex} of an oscillator circuit." Similarly, we can define Q_L of an oscillator by

$$Q_L = Q_{L,c}\sin(\Theta-\theta) = \frac{\omega_0|Z'(\omega_0)|}{2R_0}\sin(\Theta-\theta) \tag{16}$$

and, by introducing circuit efficiency η_{21}, as explained in the Appendix, we have

$$Q_L/Q_{ex} = Q_{L,c}/Q_{ex,c} = \eta_{21} = P_o/P_c \tag{17}$$

where $P_c=R_0A_0^2/2$ is the carrier power generated by the active device and P_o is the output power dissipated in R_L.

Combining (5), (7), (13), and (14), we finally obtain the generalized Edson's equations:

$$(N/C)_{AM,DSB} = \frac{4(N_e+N_{Re})B}{P_c}\cdot\frac{1}{(s^2+r^2)\sin^2(\Theta-\theta)+(2Q_L\omega_m/\omega_0)^2} \tag{18}$$

$$\Delta f_{rms} = \frac{f_0}{Q_L}\sqrt{\frac{(N_e+N_{Xe})B}{P_c}} \tag{19}$$

where $N_e=\xi N$, $N_{Re}=\xi N_R$, $N_{Xe}=\xi N_X$, and

$$\xi = \frac{(s^2+r^2)\sin^2(\Theta-\theta)+(2Q_L\omega_m/\omega_0)^2}{(s^2+r^2)\sin^2(\Theta-\theta)+(2Q_{L,c}\omega_m/\omega_0)^2}$$
$$N = |e|^2/2R_0$$

$$N_R = \frac{1}{4R_0}\left[S_{n_R}(f_m)\sin^2\Theta + S_{n_X}(f_m)\cos^2\Theta + \mathrm{Re}\{S_{n_Rn_X}(f_m)\}\sin 2\Theta\right]$$

$$N_X = \frac{1}{4R_0}\frac{1}{1+\zeta}\left[S_{n_R}(f_m)\{\cos^2\Theta+\zeta\sin^2\Theta\} + S_{n_X}(f_m)\{\sin^2\Theta+\zeta\cos^2\Theta\} - (1-\zeta)\,\mathrm{Re}\{S_{n_Rn_X}(f_m)\}\sin 2\Theta - \frac{\omega_0\sqrt{s^2+r^2}}{Q_{L,c}\omega_m}\mathrm{Im}\{S_{n_Rn_X}(f_m)\}\cos(\Theta-\theta)\right]$$

$$\zeta = \frac{(s^2+r^2)\cos^2(\Theta-\theta)}{(s^2+r^2)\sin^2(\Theta-\theta)+(2Q_{L,c}\omega_m/\omega_0)^2}.$$

The parameter ξ is introduced here so as to make the forms of (18) and (19) resemble those of the familiar Edson's equations [1]. Note that if $\sqrt{s^2+r^2}\sin(\Theta-\theta)$

$\gg 2Q_{L,c}\omega_m/\omega_0$ holds, $N_e=N$, $N_{Re}=N_R$, and $N_{Xe}=N_X$, since $\xi=1$.

N, N_R, and N_X have the dimension of watt/hertz. N is the available noise power density of white-noise source within the device. N_R and N_X are the effective available power densities of $1/f$ noise originating from the low-frequency fluctuations of the resistance and reactance of the device and circuit. If Θ is not equal to $\pi/2$, N_R and N_X include both contributions from $n_R(t)$ and $n_X(t)$. As pointed out by Hines [13] and reported by Josenhans [1] on Si Read diodes, noise sources are, in general, dependent on large signal conditions, i.e., N, N_R, and N_X will be affected by the resistive loading on the device. We have $s=2$ when the device delivers maximum power [13], since $d(R(A)A^2)/dA=0$ at power maximum. However, the saturation factor s first introduced by Edson [6] is now replaced by $\sqrt{s^2+r^2}\sin(\Theta-\theta)$ in the generalized Edson's equations. The latter includes a nonlinearity saturation factor r of the large-signal device reactance, as well as s of the negative resistance and a sine function of the angle between the device and circuit impedance line [9].

For the simplest case in Fig. 1(b), that is, $\overline{X}(A)=0$ and $Z(\omega)=R_i+R_L+j(\omega L-1/\omega C)$, we have $r=0$, $Z'(\omega_0)=2jL$ or $\theta=0$, and $\Theta=\pi/2$. Edson's equations (18) and (19) then become

$$(N/C)_{\mathrm{AM,DSB}}=\frac{4(N+N_R)B}{P_c}\,\frac{1}{s^2+(2Q_L\omega_m/\omega_0)^2}$$

$$\Delta f_{\mathrm{rms}}=\frac{f_0}{Q_L}\sqrt{\frac{(N+N_X)B}{P_c}}$$

where $N=|e|^2/2R_0$, $N_R=S_{n_R}(f_m)/4R_0$, $N_X=S_{n_X}(f_m)/4R_0$, and $Q_L=\omega_0L/(R_i+R_L)$ [14]. Furthermore, if we can neglect circuit loss, i.e., $Q_L=Q_{ex}$, and $1/f$ noise, the above equations reduce to those described by Josenhans [1].

III. Noise-Measurement Method

A block diagram of the noise-measuring system at X band is shown in Fig. 2. Although the system is essentially the same as reported by Ashley *et al.* [15] and Ondria [16], fairly detailed descriptions of the method are presented here in order to show that measurements in a relatively wide range of frequency off carrier from 1 kHz to 10 MHz can be performed with a careful calibration of the frequency response of the detectors, and evaluation of loaded Q of the cavity resonator enables one to make FM measurements continuously from 1 kHz to beyond the half-power frequency points of the cavity.

In AM noise measurement, path 1 in Fig. 2 is used with the waveguide shorting switch closed and path 2 is made at a maximum attenuation. Path 2 alone, of course, may be used instead. The oscillator output is fed into the H-arm of the magic tee balanced detectors, each of which contains a GaAs Schottky-barrier diode in a modified 1N23-type package. Each diode is loaded

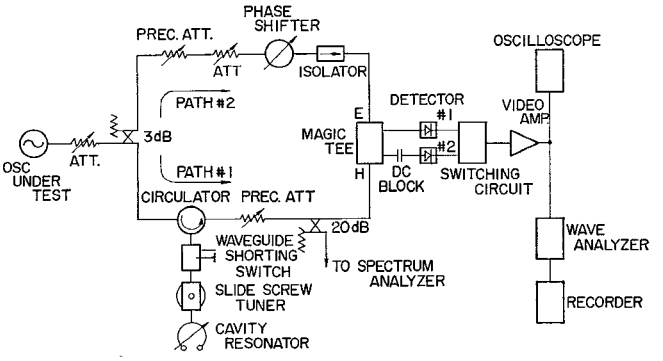

Fig. 2. Block diagram of AM and FM noise-measuring system.

by a metal thin-film resistor of 10 kΩ and a stray capacitance of about 140 pF. Input power to each detector is typically 1∼5 dBm and the two detector mounts are adjusted so as to have detector characteristics as identical as possible. This adjustment can be performed relatively easily by monitoring two detected dc outputs on an X–Y recorder. One of the detector mounts is dc blocked from the magic tee by a 0.5-mm thick Teflon sheet so that the two outputs can be electrically switched to obtain their sum or difference, thereby enabling us to cancel out system noise. Especially, the dc isolated mount is electrically shielded to avoid power-line and other radio-frequency pickup. The output of the switching circuit is then fed into a low-noise video amplifier that has an input impedance of 200 kΩ and a flat gain of 40 dB from 300 Hz to 2 MHz. The frequency components of the output are measured with a tunable wave analyzer. Since the meter indication usually fluctuates, the output of the analyzer is read on a recorder.

If the output waveform of the oscillator under test is represented by (1), the ac component of the output voltage from each detector is given by

$$v_i=CV_{\mathrm{dc}}a(t)+v_{ni},\qquad i=1,2$$

where V_{dc} is the dc output voltage, v_{ni} is the noise voltage originating from each detector diode, and C is the correction factor defined by Ashley *et al.* [15]. The GaAs Schottky-barrier diodes employed exhibited least noise around $V_{\mathrm{dc}}=1.2$ V and $C=1.47$ was typically obtained. C is evaluated from "V_{dc} versus normalized RF voltage" curve [15]. It is, however, frequency dependent because of a stray capacitance C_s. By simple calculations, the frequency dependence of C is given by

$$C(f)=C(0)/\sqrt{1+(f/f_c)^2} \tag{20}$$

where $C(0)$ denotes the dc value of C and $f_c=(1/2\pi C_s)\cdot(1/R_v+1/R)$. R_v and R are the video and load resistances of the diode, respectively. From $R=10$ kΩ, $C_s=140$ pF, and $R_v=1$ kΩ measured by a dc method, $f_c=800$ kHz is anticipated. On the other hand, $C(f)$ was experimentally evaluated by applying an amplitude modulated CW signal to detectors and taking the ratio

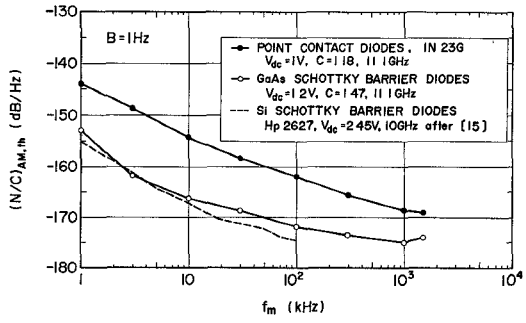

Fig. 3. AM threshold for GaAs Schottky-barrier diodes and Si point contact diodes (1N23G) compared with that of Si Schottky-barrier diodes [15].

of the outputs with $R=10$ kΩ and 50 Ω. Since $f_c \gtrsim 20$ MHz is expected for $R=50$ Ω, the ratio will be proportional to $C(f)$ for $f \lesssim 10$ MHz. $C(f)$ thus obtained was found to be approximately expressed by (20) with $f_c=700$ kHz. The unbalance of the two detectors was also evaluated to be less than −20 dB from 1 kHz to 10 MHz by taking the ratio of the sum to the difference of their outputs.

Corresponding to the sum and difference of the detector outputs, the rms voltages measured with the wave analyzer at frequency f_m in a bandwidth B are represented by

$$V_m(f_m) = G(f_m)\sqrt{S_{v_m}(f_m)B}$$
$$V_{th}(f_m) = G(f_m)\sqrt{S_{v_{th}}(f_m)B}$$

where $G(f_m)$ is the voltage gain of the amplifier, $S_{v_m}(f_m)$ and $S_{v_{th}}(f_m)$ are the power spectral densities of $v_m=v_1+v_2+v_{na}=2CV_{dc}a(t)+v_{n_1}+v_{n_2}+v_{na}$ and $v_{th}=v_1-v_2+v_{na}=v_{n_1}-v_{n_2}+v_{na}$, respectively, and v_{na} is the equivalent input noise voltage of the amplifier. Hence, in a 1-Hz bandwidth basis, we have

$$(N/C)_{AM,DSB} = 2S_a(f_m) = \frac{V_m^2(f_m) - V_{th}^2(f_m)}{4C^2(f_m)V_{dc}^2G^2(f_m)B} \quad (21)$$

since $a(t)$, v_{n_1}, v_{n_2}, and v_{na} are incoherent. A measure of the system sensitivity $(N/C)_{AM,th}$, is termed the AM threshold [15] and is obtained by substituting $V_m^2(f_m)=2V_{th}^2(f_m)$ in (21). When a high-Q Gunn oscillator was employed as a signal source, the GaAs Schottky-barrier diodes used exhibited $(N/C)_{AM,th}$ as low as that of Si Schottky-barrier diodes [15], as shown in Fig. 3 together with $(N/C)_{AM,th}$ for Si point contact diodes 1N23G. The value of $(N/C)_{AM,DSB}$ less than $(N/C)_{AM,th}$ can be evaluated by (21) with less accuracy.

In FM noise measurement, power from the oscillator under test is divided into paths 1 and 2. In path 1, called the signal channel, the carrier is suppressed by more than 40 dB with a very nearly critically coupled high-Q cavity resonator tuned to f_0, and the reflected noise sidebands are fed into the magic tee balanced detectors. Path 2, called the reference channel, is used to give the detectors the reference carrier for demodulation of the FM noise sidebands fed from the signal channel. If the phase difference ϕ_R between the signal and reference channels is adjusted as $|\sin\phi_R|=1$ by means of the phase shifter, the difference of the output voltage from the two detectors is proportional to rms frequency deviation with AM noise being suppressed [15], [16]. Furthermore, by using narrow-band noise expressions for $a(t)$ and $\phi(t)$ in (1), one can easily show that the rms component of the difference voltage at frequency f_m in bandwidth B is expressed by

$$v_{o,rms} = \frac{S}{\sqrt{1+(2Q_L\delta_m)^2}}\Delta f_{rms}$$

where Δf_{rms} is the rms frequency deviation in bandwidth B around $\pm f_m$ off carrier, $\delta_m=f_m/f_0$, Q_L is the loaded Q of the cavity, and S is a constant of the system proportional to $[Q_Lf_0^{-1}]\times$[power input to path 1]$^{1/2}$. Since the frequency response of the detectors is proportional to $C(f_m)/C(0)$, as in the AM measurement, the wave analyzer reading $V_{o,rms}$ is equal to $v_{o,rms}$ multiplied by $C(f_m)/C(0)$ and $G(f_m)$. Thus we have

$$\Delta f_{rms} = \frac{C(0)}{C(f_m)}\frac{\sqrt{1+(2Q_L\delta_m)^2}}{S}\frac{V_{o,rms}}{G(f_m)}. \quad (22)$$

Δf_{rms} in a 1-Hz basis is obtained by dividing the right-hand side of the above equation with $\sqrt{B}$. If $V_{o,rms}$ is comparable to the system noise, it should be replaced by $\sqrt{V_{o,rms}^2-V_{th,rms}^2}$ as in AM measurements, where $V_{th,rms}$ is the analyzer reading with the signal channel attenuator being adjusted at a maximum attenuation [15]. Usually, the measured $V_{o,rms}$ was greater than $V_{th,rms}$ by more than 20 dB. Q_L was measured by a swept-frequency technique viewing the reflected wave from the cavity on a spectrum analyzer with the cavity *in situ* and found to be ~9000 typically. Since the cavity was almost critically coupled by means of a slide screw tuner, the half-power frequency points were easily found from the intersection of a doubly exposed spectrum photograph taken with the cavity at resonance and detuned. In the detuned case, the reflected wave was attenuated by 3 dB by means of the precision attenuator. S was calibrated at a frequency where $2Q_L\delta_m \ll 1$ by the carrier null method [15], using a varactor-tuned Gunn oscillator. During this calibration, ϕ_R was adjusted to obtain the maximum analyzer reading. Once Q_L and S have been found, Δf_{rms} can be evaluated continuously with (22) for a frequency from near carrier to beyond the half-power frequency points.

The accuracy of the measurement was estimated to be ±1 dB for $(N/C)_{AM,DSB}$ and ±10 percent for Δf_{rms}.

IV. Results and Discussions

Noise measurements have been performed on X-band Gunn and avalanche diode (Si and GaAs) oscillators for frequency off carrier from 1 kHz to 1.5 MHz, or sometimes to 10 MHz, with the previously described method. The diodes used are mounted in prong-type packages,

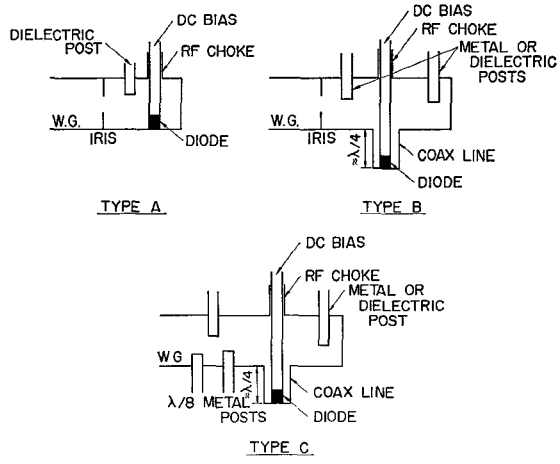

Fig. 4. Various types of circuits used for Gunn and avalanche oscillators.

the ceramic portion of which has an outer diameter of 2 mm and a height of 1 mm. The various oscillator circuits employed are schematically shown in Fig. 4. The AM and FM noise spectra are given in a 1-Hz bandwidth by reducing the data measured in a bandwidth of $B = 200$ Hz, 1 kHz, or 3 kHz.

A. Gunn Oscillators

The Gunn diodes (Toshiba S3020 and S8201) have a n^{++}-n-n^{+} sandwich structure made from epitaxially grown n–GaAs. The n^{++} layer was formed by liquid-phase epitaxy on the n-n^{+} epitaxial wafer grown in vapor phase.

Fig. 5 shows AM and FM noise spectra of three Gunn oscillators with different Q_{ex} values. FM noise measurement was extended to 8 MHz for the oscillator ②. These oscillators contained the same diode, whose active layer is 9 μm and doped to about 8×10^{14} cm^{-3}. The oscillator circuits are type A for ② and ③ and type C for ① (see Fig. 4). The diode was operated at a constant bias voltage of 10 V around which the output power reaches a maximum. The operating current in each oscillator was also made equal to 0.63 A by circuit adjustments so as to keep the resistive loading seen from the diode chip terminal as identical as possible, since the dc current through a Gunn diode is experimentally known to be a sensitive parameter for the loading conditions. Q_{ex} of the oscillators was measured from the frequency pulling by inserting a slide screw tuner (VSWR = 1.2) between the matched load and the oscillator. The evaluation formula for Q_{ex} is shown in the Appendix, Section D. Q_{ex} thus measured agreed with that measured from injection locking (see the Appendix, Section C) within 10 percent in the case of oscillator ①.

Much improvement in FM noise is observed with the increase of Q_{ex}, as shown in Fig. 5, while the AM noise spectra do not change appreciably and have very low values comparable to $(N/C)_{AM,th}$ (see Fig. 3). For $f_m \lesssim 100 \sim 200$ kHz, modulation noise or $1/f$ noise predominates in both AM and FM. Above $f_m \gtrsim 300 \sim 500$ kHz, both noise spectra become white, showing that RF noise or white noise is dominant. Especially curve ② in Fig. 5(b) indicates that Δf_{rms} is nearly constant to 8 MHz. If we assume the frequency dependence of the noise spectra in the form

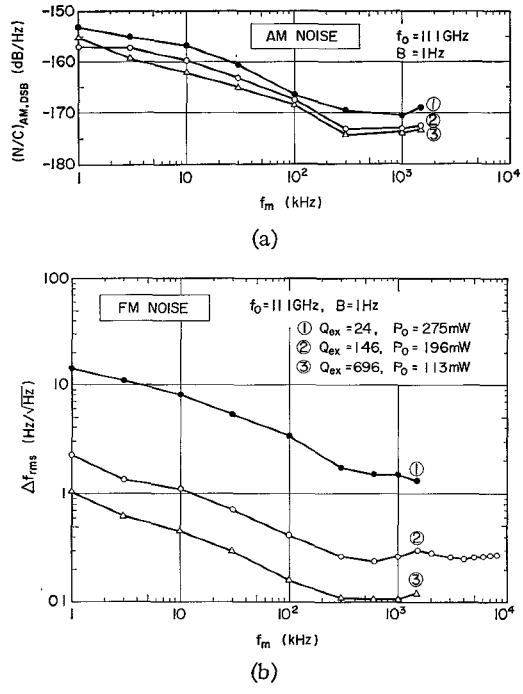

Fig. 5. Measured noise spectra of three Gunn oscillators containing the same diode and with different Q_{ex}. The diode was biased to 10 V and 0.63 A. (a) AM noise spectra. (b) FM noise spectra.

$$(N/C)_{AM,DSB} \propto 1 + (f_R/f_m)^{\mu} \tag{23}$$

$$\Delta f_{rms} \propto [1 + (f_X/f_m)^{\nu}]^{1/2} \tag{24}$$

where μ and ν are constants and f_R and f_X represent "noise corner" frequencies, we obtain

$$\mu \approx 0.8$$

$$\nu \approx 0.9$$

$$f_R = 100 \sim 160 \text{ kHz}$$

$$f_X = 190 \sim 230 \text{ kHz}$$

by approximately fitting the curves in Fig. 5. The constants μ and ν are nearly equal to 1, indicating that the noise spectra approximately follow the $1/f$ law for $f_m < f_R$ or f_X.

The output power to the load P_o decreased with the increase of Q_{ex}, as seen from the inset of Fig. 5(b). On the other hand, the carrier power P_c would not change regardless of Q_{ex} if the resistive loading on the diode chip terminal is equal. This is what was expected by adjusting the bias voltage and current equal in each oscillator of Fig. 5. P_o, however, is given by

$$P_o = \eta_{21} P_c = (Q_L/Q_{ex}) P_c \tag{25}$$

as described in the Appendix, where η_{21} is the circuit efficiency. If we assume that P_c is constant for the oscillator

TABLE I
NOISE PARAMETERS OF GUNN OSCILLATORS

No.	f_0 (GHz)	P_o (mW)	Q_{ex}	$\partial f_0/\partial V$ (MHz/V)	$Q_L^{(1)}$	$Q_L^{(2)}$	Δf_{rms} (Hz/$\sqrt{Hz}$)	$(N/C)_{AM,DSB}$ (dB/Hz)	μ	ν	f_R (kHz)	f_X (kHz)	N/kT_0 (dB)	$\sqrt{s^2+r^2}\sin(\Theta-\theta)$
①	11.1	275	24	-20	24	24	1.53	-170.5	0.8	0.85	100	230	29	2.2
②	11.1	196	146	-4.3	104	113	0.27	-173.0	0.8	0.87	160	190	27	2.5
③	11.1	113	696	-1.6	286	300	0.10	-173.6	0.83	0.91	160	200	27	2.6
④	11.1	120	780	—	320	—	0.056	-176.5	0.8	0.85	400	140	23	2.0
⑤	9.4	125	136	—	136	—	0.03	-170.5	0.75	0.94	350	280	28	2.9

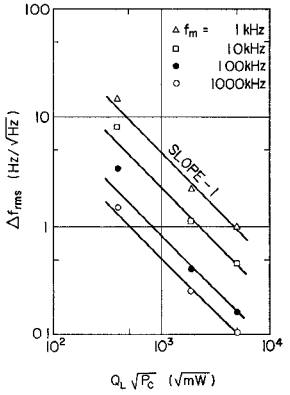

Fig. 6. Plots of Δf_{rms} versus $Q_L\sqrt{P_c}$ for the oscillators of Fig. 5. $Q_L^{(2)}$ in Table I is employed as Q_L.

①~③ and P_c is equal to P_o, i.e., $Q_L = Q_{ex}$ for ①, we have $P_c = 275$ mW for ② and ③ and, by (25), $Q_L = 104$ and 286 for ② and ③, respectively. Let us denote these Q_L by $Q_L^{(1)}$. Meanwhile, the voltage pushing figure of an oscillator frequency is, in general, inversely proportional to Q_L. Assuming again $Q_L = Q_{ex} = 24$ for ①, we can evaluate Q_L [denoted by $Q_L^{(2)}$] for ② and ③ from the measured pushing figures. $Q_L^{(1)}$ and $Q_L^{(2)}$ are given in Table I from which they are seen to agree with each other within 10 percent. From this, we can safely say that $P_c = 275$ mW in oscillators ①~③.

By keeping the resistive loading on the diode as identical as possible, it is expected that N, N_R, N_X, and $\sqrt{s^2+r^2}\sin(\Theta-\theta)$ described in Section II are almost unchanged for oscillators ①~③, provided that Θ does not vary appreciably. Then the generalized Edson's equations (18) and (19) predict that, to the first order, $\Delta f_{rms} \propto Q_L^{-1}P_c^{-1/2}$ and $(N/C)_{AM,DSB}$ is independent of Q_L if $f_m \ll f_0\sqrt{s^2+r^2}\sin(\Theta-\theta)/2Q_L$. The log–log plots of measured Δf_{rms} (of Fig. 5) versus $(Q_L\sqrt{P_c})$ are shown in Fig. 6, where $Q_L^{(2)}$ was used for Q_L since the voltage pushing seems to be less sensitive to the loading conditions. From this, we find that $\Delta f_{rms} \propto Q_L^{-1}P_c^{-1/2}$ nearly holds. On the contrary, the AM noise does not vary appreciably with Q_L, as seen from Fig. 5(a), indicating $\sqrt{s^2+r^2}\sin(\Theta-\theta) \gg 2Q_Lf_m/f_0$ for $f_m = 1.5$ MHz.

To check whether the measured Δf_{rms} may arise from a modulation by voltage fluctuations in the power supply (hp is 6101 A) or not, the bias voltage fluctuations ΔV_{rms} were measured. The rms frequency modulation calculated from ΔV_{rms} times the voltage pushing figure was found to be an order of magnitude smaller than the measured Δf_{rms} shown in Fig. 5.

Let us now evaluate N_e, N_{Re}, N_{Xe}, and $\sqrt{s^2+r^2}\cdot\sin(\Theta-\theta)$ from the measured noise data using Edson's equations (18) and (19). Since $\sqrt{s^2+r^2}\cdot\sin(\Theta-\theta) \gg 2Q_Lf_m/f_0$, we have $\xi = 1$. Hence, $N = N_e$, $N_R = N_{Re}$, and $N_X = N_{Xe}$. Substituting Δf_{rms} of Fig. 5(b) at $f_m = 1$ MHz, where the white noise predominates, i.e., $N \gg N_X$, into (19), we obtain N. Then substituting $N(\gg N_{Re})$ and measured $(N/C)_{AM,DSB}$ into (18) we have $\sqrt{s^2+r^2}\sin(\Theta-\theta)$. N divided by kT_0 (−174 dB/Hz), called the effective noise-temperature ratio for white noise, where T_0 is the standard noise temperature (290°K), is 27~29 dB and $\sqrt{s^2+r^2}\sin(\Theta-\theta)$, the effective saturation factor, is 2.2~2.6, as shown in Table I. Since $(N/C)_{AM,DSB}$ and Δf_{rms} are approximately expressed by experimental formulas (23) and (24), we have

$$N_R \approx N(f_R/f_m)^\mu$$
$$N_X \approx N(f_X/f_m)^\nu.$$

The values of μ, ν, f_R, and f_X for each oscillator are given in Table I.

Sweet and MacKenzie [17] have observed that FM noise of their Gunn oscillator consisted of both $1/f$ and white components. From their results, $N/kT_0 \approx 15$ dB and $f_X \approx 4$~40 kHz are inferred, indicating their diode is very quiet. Their results also imply that N_X is a sensitive function of voltage pushing figures which may be controlled by the resistive loading, as well as the bias condition.

Noise spectra of other Gunn oscillators are shown in Fig. 7 with that of klystron 2K25 (Toshiba) for comparison. The diode in the oscillator ④ belongs to the same lot as that of Fig. 5. The diode in ⑤ has an active layer about 10~11 μm thick and is doped to $\sim 1\times10^{15}$ cm^{-3}. The various noise parameters derived by the same procedure as above are given in Table I. Although the Gunn oscillators exhibit more AM noise near carrier than the klystron, they become less noisy by more than 5 dB at $f_m \gtrsim 1$ MHz.

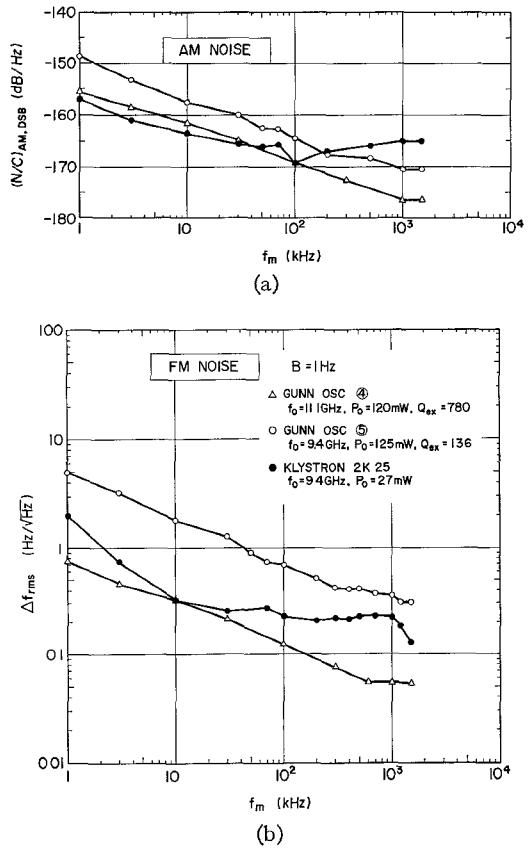

Fig. 7. Measured noise spectra of another Gunn oscillator and klystron 2K25 (Toshiba). Bias conditons are 11 V, 0.62 A for ④ and 9 V, 0.49 A for ⑤. (a) AM noise spectra. (b) FM noise spectra.

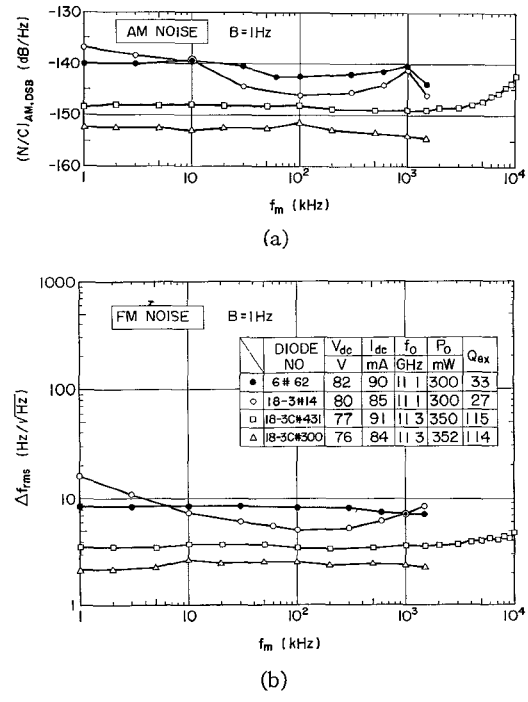

Fig. 8. Measured noise spectra of Si avalanche oscillators. (a) AM noise spectra. (b) FM noise spectra.

In applications such as local oscillators for mixers, the AM noise component of the local oscillator degrades the mixer noise figure. The noise-figure degradation due to LO noise of a single-ended mixer is given by [18]

$$F_2 - F_1 = \frac{P_{LO}(N/C)_{AM,DSB}}{2kT_0} \tag{26}$$

where P_{LO} is the LO power fed into the mixer, $(N/C)_{AM,DSB}$ is the value in a 1-Hz bandwidth at $f_m = f_{IF}$, and F_2, F_1 are DSB noise figure of the mixer with the noisy LO and the noiseless one, respectively. For the Gunn oscillator ⑤, 10 log $(F_2/F_1) = 4.6$ dB is expected from (26) using the $(N/C)_{AM,DSB}$ calculated from (18) with $\xi \approx 1$, $F_1 = 3$ dB, $f_{IF} = 70$ MHz, and $P_{LO} = 5$ mW. For the klystron 2K25, the corresponding degradation is calculated to be 10.2 dB if we use the $(N/C)_{AM,DSB}$ at 1 MHz. Meanwhile, the degradation was measured in a single-ended mixer ($f_{IF} = 70$ MHz, $F_1 = 3$ dB) and was found to be 6.2 dB for the Gunn oscillator ⑤ and 9 dB for the klystron at $P_{LO} = 5$ mW. F_1 was evaluated with (a Gunn oscillator) + (a high-Q bandpass filter) configuration. The agreement between the measured and calculated values is fairly good. Thus once the noise parameters have been evaluated, we can predict the noise degradation of a single-ended mixer by use of (18) and (26). Recently developed Gunn oscillators exhibit 10 log $(F_2/F_1) \lesssim 0.5 \sim 1$ dB because of the improvement in the device fabrication and a high-Q low-loss circuit design.

B. Avalanche Oscillators

Noise spectra of Si and GaAs avalanche oscillators have also been measured. The Si avalanche diode (Toshiba S3019) has a p^+-n-n^+ structure made by boron diffusion into an epitaxially grown n-n^+ wafer. The junction diameters are ~140 μm, and the breakdown voltages of the diodes used were 67~68 V. The GaAs avalanche diodes recently developed in our laboratory are capable of operation at an efficiency as high as 12~13 percent [19]. They are made by Zn diffusion into an n–GaAs epitaxial wafer by an open-tube method. The tested diodes have a breakdown voltage of 46~49 V and a junction diameter of about 90 μm.

Fig. 8 shows AM and FM noise spectra of Si avalanche oscillators. The diodes 18-3C#431 and 18-3C#300 were operated in the type-B circuit and the rest in the type C (see Fig. 4). Contrary to the case of the Gunn oscillators, the Si avalanche oscillators exhibit almost flat spectra, except for the diode 18-3#14. According to Scherer [3], the AM noise of avalanche oscillators arising from the modulation by white appearing low-frequency current fluctuations can be greatly suppressed below the RF noise level by making the bias circuit impedance high. We have also observed about 4 dB variation in AM noise by changing the bias circuit impedance, and found that the AM noise reaches a minimum if a resistance of more than 100 Ω is connected in series to the dc power supply (hp is 6106 A) employed in a current-limiting state. Thus we operated all the diodes in this condition. The gradual increase in AM noise of the diode 18-3C#431 for $f_m \gtrsim 3$ MHz may be

TABLE II
NOISE PARAMETERS OF AVALANCHE OSCILLATORS

Material	Diode No.	f_0 (GHz)	P_o (mW)	Q_{ex}	Δf_{rms} (Hz/$\sqrt{Hz}$)	$(N/C)_{AM,DSB}$ (dB/Hz)	μ	ν	f_R (kHz)	f_X (kHz)	N/kT_0 (dB)	$\sqrt{s^2+r^2}\sin(\Theta-\theta)$
Si	6#62	11.1	300	33	8.2	-142.5	—	—	<1	<1	47	0.65
Si	18-3#14	11.1	300	27	5.1	-146.0	0.55	0.72	20	14	41	0.50
Si	18-3C#431	11.3	350	115	3.6	-149.0	—	—	<1	<1	51	2.1
Si	18-3C#300	11.3	352	114	2.4	-154.0	—	—	<1	<1	47	2.4
GaAs	I19T20	11.3	350	109	1.8	-155.0	0.9	1.1	3	90	44	2.0
GaAs	I19T20	11.3	150	109	1.3	-158.0	0.9	1.1	2	60	38	2.0

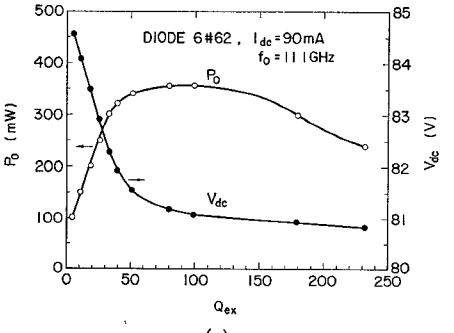

(a)

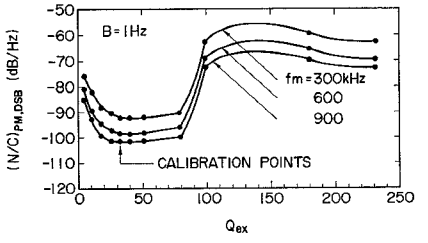

(b)

Fig. 9. (a) Dependence of output power P_o and the dc bias voltage V_{dc} of an Si avalanche oscillator on Q_{ex}. (b) Dependence of $(N/C)_{PM,DSB}$ on Q_{ex}. The diode is 6#62 of Fig. 8 and the type-C circuit (Fig. 4) was used to obtain various Q_{ex}. The calibration points mean that $(N/C)_{PM,DSB}$ was calibrated with the measured Δf_{rms} of Fig. 8(b).

attributed to the fact that the stray capacitances in the RF choke section and the bias feed cable lower the impedance as the video frequency increases. Meanwhile, the corresponding Δf_{rms} is almost flat to 10 MHz, suggesting that it is mainly composed of RF noise [3].

If we assume that the white appearing modulation noise is well suppressed and the main noise sources are white in Fig. 8, N/kT_0 and $\sqrt{s^2+r^2}\sin(\Theta-\theta)$ can be evaluated in a similar manner as in the Gunn oscillators. They are given in Table II. Carrier power P_c was considered to be equal to the output power P_o and the minimum $(N/C)_{AM,DSB}$ and corresponding Δf_{rms} were used in the above evaluation. The effective noise-temperature ratio N/kT_0 ranges from 41 to 51 dB and the effective saturation factor $\sqrt{s^2+r^2}\sin(\Theta-\theta)$ from 0.5 to 2.4.

It is often observed that noise in avalanche oscillators is very sensitive to the loading on a diode. Fig. 9(b)

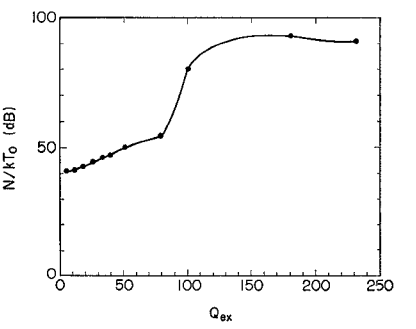

Fig. 10. Dependence of the effective noise-temperature ratio N/kT_0 on Q_{ex}.

shows the dependence of $(N/C)_{PM,DSB}$ on the coupling between the diode and load. The diode 6#62 was mounted in the type-C circuit of Fig. 4, which has three stubs, each separated by $\lambda_g/8$. With these stubs, Q_{ex} of the oscillator could be continuously varied. With the increment of Q_{ex}, P_o increased to a maximum and further increments of Q_{ex} diminished P_o, as shown in Fig. 9(a). Since decrease of dc voltage corresponds to the increase of the RF voltage across the diode chip terminal [20], the RF voltage can be considered to increase with Q_{ex} in Fig. 9. PM or FM noise near carrier generally prevails greatly over AM in free-running oscillators, and the $(N/C)_{PM,DSB}$ was obtained by observing the output power spectra on a spectrum analyzer that has a calibrated dynamic range in excess of 60 dB. The spectra in the IF bandwidth of 10 kHz were recorded on an X-Y recorder and calibration of $(N/C)_{PM,DSB}$ was performed at the "calibration points" indicated in Fig. 9(b) from the corresponding Δf_{rms} of Fig. 8(b). Using (8) and (19), N/kT_0 were calculated with $\xi=1$, $N_X \ll N$, $Q_L = Q_{ex}$, and $P_c = P_o$. They are shown in Fig. 10. The effective noise-temperature ratio is seen to increase with Q_{ex} or the RF voltage amplitude across the diode chip terminal, and it suddenly increases near the output power maximum. Such a phenomenon is often observed in another avalanche diode, and it imposed a severe restriction on the circuit design of the oscillators.

An amplifier was constructed earlier using the same diode 6#62, and the DSB noise figure of 37~40 dB was obtained at 10.8~11.8 GHz at an average gain of 7 dB [21]. Since the optimum noise measure M of an ampli-

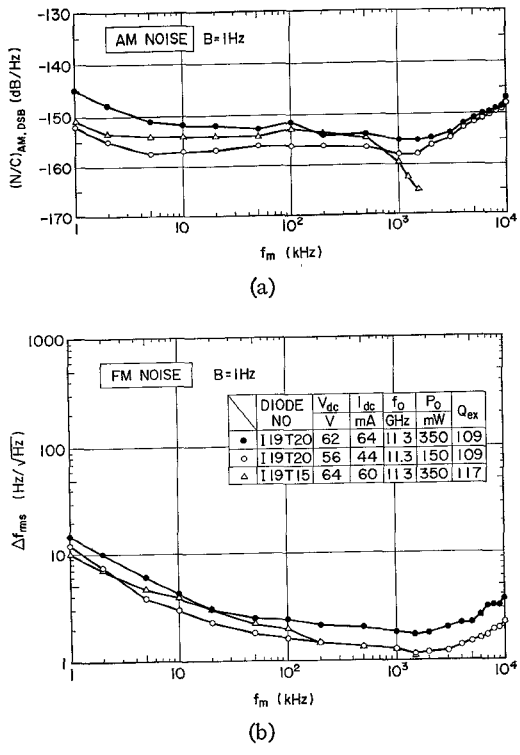

Fig. 11. Measured noise spectra of GaAs avalanche oscillators. (a) AM noise spectra. (b) FM noise spectra.

fier built with a device which has an effective noise temperature ratio N/kT_0 is given by [8]

$$M = (F - 1)/(1 - 1/G) = N/kT_0$$

we obtain $N/kT_0 = 38 \sim 41$ dB at small signal conditions. These values are consistent with those of Fig. 10 at small Q_{ex} or small RF voltage.

Noise spectra of GaAs avalanche oscillators are shown in Fig. 11. The diodes were mounted in the type-B circuit. The remarkable differences in oscillator characteristics, as compared with the Si avalanche oscillators, were that the GaAs diodes were operated at about twice higher efficiency than the Si diodes and the frequency pushing by the bias current was about an order of magnitude larger than the Si, i.e., $1.2 \sim 1.9$ MHz/mA for the diodes shown in Fig. 11. The presence of modulation noise is remarkable in the GaAs avalanche oscillators. This may correspond to the large pushing figures. The gradual rise of both AM and FM noise for $f_m \gtrsim 3$ MHz may be attributed to the decrease of the bias circuit impedance as in the Si avalanche diodes. When the bias current was made smaller, reduction of AM and FM noise was observed in the diode I19T20. The rapid decrease of AM noise around $f_m \approx 1$ MHz in I19T15 is anomalous and not understood yet. This phenomenon was also observed in another diode. N/kT_0 and $\sqrt{s^2+r^2} \cdot \sin(\Theta - \theta)$ were evaluated at f_m of minimum AM noise and are shown in Table II, together with other parameters. Though the effective noise–temperature ratio is several decibels smaller than those of Si diodes, the presence of $1/f$ noise makes the AM and FM noise near a carrier larger than Si diodes. Future progress in GaAs device technology may diminish the $1/f$ noise component.

V. Conclusions

The generalized Edson's equations that express AM noise-to-carrier ratio and rms frequency deviation in terms of the suitably defined circuit and device parameters have been derived for a generalized model of a negative-resistance oscillator from Kurokawa's theory [9]. They have similar forms as those of an oscillator with a simple LCR circuit, but include effective available noise power densities of $1/f$ noise, as well as white noise, an effective saturation factor, and a suitably defined Q_L of the oscillator.

AM and FM noise spectra of X-band Gunn oscillators and Si or GaAs avalanche oscillators have been measured for frequency off carriers extending from 1 kHz to 1.5 MHz (sometimes to 10 MHz) by using the method reported by Ashley *et al.* [15] successfully to measure AM noise as low as 175 dB/Hz below the carrier at $f_m = 1$ MHz with GaAs Schottky-barrier diodes.

The validity of the generalized Edson's equations has been verified for Gunn oscillators from the dependence of noise on Q_L. An effective noise–temperature ratio N/kT_0 for white noise and an effective saturation factor $\sqrt{s^2+r^2} \sin(\Theta - \theta)$ have been evaluated from the measured $(N/C)_{AM,DSB}$ and Δf_{rms} using the generalized Edson's equations. The Gunn, Si avalanche, and GaAs avalanche oscillators have $N/kT_0 = 23 \sim 29$, $41 \sim 51$, and $38 \sim 44$ dB and $\sqrt{s^2+r^2} \sin(\Theta - \theta) = 2 \sim 2.9$, $0.5 \sim 2.4$, and 2, respectively. The $1/f$ noise has been found to be dominant near carrier in Gunn and GaAs avalanche oscillators, and the parameters for $1/f$ noise have been evaluated approximately. It has been observed that N/kT_0 in an Si avalanche diode gradually increases with the RF voltage across the diode chip terminal and suddenly degrades near an output power maximum.

Appendix

A. Preliminary Theorem

Presume pure resistances R_1 and R_2 to be coupled via a reciprocal circuit, as shown in Fig. 12. If the equations

$$Z_1(\omega_0) = -R_1 \tag{A1}$$

$$Z_2(\omega_0) = -R_2 \tag{A2}$$

are satisfied at $\omega = \omega_0$, where $Z_1(\omega)$ and $Z_2(\omega)$ are the impedances looking into ports 1-1′ and 2-2′, respectively, then the following equality holds:

$$\frac{|Z_1'(\omega_0)|}{-R_1} = \eta_{21} \frac{|Z_2'(\omega_0)|}{R_2} \tag{A3}$$

where $Z_i'(\omega_0) = [dZ_i(\omega)/d\omega]_{\omega=\omega_0}$, $i = 1$, 2, and η_{21} is de-

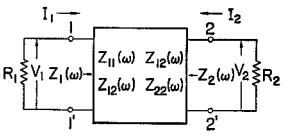

Fig. 12. Reciprocal circuit that couples pure resistances R_1 and R_2.

fined and given by

$$\eta_{21} = (\text{power dissipated by } R_2)/(\text{power generated by } R_1) = -\frac{R_2}{R_1}\left|\frac{R_1 + Z_{11}(\omega_0)}{R_2 + Z_{22}(\omega_0)}\right|. \quad \text{(A4)}$$

Especially for a lossless coupling circuit, i.e., Z_{11}, Z_{22}, and Z_{12} are purely imaginary [22], $\eta_{21}=1$.

Proof: From the definition of the impedance matrix we have [22]

$$Z_i(\omega) = Z_{ii}(\omega) - \frac{Z_{12}^2(\omega)}{Z_{jj}(\omega) + R_j} = \frac{D(\omega) + R_j Z_{ii}(\omega)}{R_j + Z_{jj}(\omega)}, \quad (i, j) = (1, 2) \text{ or } (2, 1) \quad \text{(A5)}$$

where $D(\omega) = Z_{11}(\omega)Z_{22}(\omega) - Z_{12}^2(\omega)$. At $\omega=\omega_0$ we obtain

$$[R_1 + Z_{11}(\omega_0)][R_2 + Z_{22}(\omega_0)] = Z_{12}^2(\omega_0) \quad \text{(A6)}$$

$$[D(\omega_0) + R_1 Z_{22}(\omega_0)]/[R_1 + Z_{11}(\omega_0)] = -R_2 \quad \text{(A7)}$$

$$[D(\omega_0) + R_2 Z_{11}(\omega_0)]/[R_2 + Z_{22}(\omega_0)] = -R_1 \quad \text{(A8)}$$

from (A1) and (A2). Let P_1 and P_2 be the power generated and dissipated in R_1 and R_2, respectively, at $\omega=\omega_0$. They are given by

$$P_1 = \frac{1}{4}(V_1 I_1^* + V_1^* I_1) = -\frac{R_1}{2}|I_1|^2$$

$$P_2 = \frac{1}{4}(-V_2 I_2^* - V_2^* I_2) = \frac{R_2}{2}\left|\frac{R_1 + Z_{11}(\omega_0)}{Z_{12}(\omega_0)}\right|^2 |I_1|^2.$$

Using (A6), we obtain (A4):

$$\eta_{21} = \frac{P_2}{P_1} = -\frac{R_2}{R_1}\left|\frac{R_1 + Z_{11}(\omega_0)}{Z_{12}(\omega_0)}\right|^2 = -\frac{R_2}{R_1}\left|\frac{R_1 + Z_{11}(\omega_0)}{R_2 + Z_{22}(\omega_0)}\right|.$$

Meanwhile, differentiation of (A5) gives

$$Z_i'(\omega) = [\{D'(\omega) + R_j Z_{ii}'(\omega)\}\{R_j + Z_{jj}(\omega)\} - Z_{jj}'(\omega)\{D(\omega) + R_j Z_{ii}(\omega)\}]/[R_j + Z_{jj}(\omega)]^2.$$

Using (A7) and (A8) we have at $\omega=\omega_0$

$$\frac{Z_1'}{Z_2'} = \left(\frac{R_1+Z_{11}}{R_2+Z_{22}}\right)^2 \cdot \left[\frac{(D'+R_2Z_{11}')(R_2+Z_{22}) - Z_{22}'(D+R_2Z_{11})}{(D'+R_1Z_{22}')(R_1+Z_{11}) - Z_{11}'(D+R_1Z_{22})}\right] = \frac{R_1+Z_{11}}{R_2+Z_{22}} \quad \text{(A9)}$$

where abbreviations like $Z_1' = Z_1'(\omega_0)$, $Z_2' = Z_2'(\omega_0)$, etc., are employed. From (A4) and (A9), (A3) is obtained. If Z_{11}, Z_{22}, and Z_{12} are purely imaginary, a simple calculation gives $\eta_{21}=1$.

B. Definition of Q-Value

An oscillator represented by Fig. 1(a) is equivalent to Fig. 12 if we replace R_1, R_2, and Z_{11} by $-\overline{R}$, R_L, and $Z_{11}+j\overline{X}$, respectively. At the frequency of oscillation, (A1) and (A2) hold, i.e., $j\overline{X}(A_0)+Z(\omega_0)=\overline{R}(A_0)\equiv R_0$ and $Z_{ex}(\omega_0, A_0) = -R_L$. Since $\partial[j\overline{X}(A)+Z(\omega)]/\partial\omega = Z'(\omega)$, the previous theorem gives

$$\frac{|Z'(\omega_0)|}{R_0} = \eta_{21}\frac{|Z_{ex}'(\omega_0)|}{R_L} \quad \text{(B1)}$$

where $Z_{ex}'(\omega_0) \equiv [\partial Z_{ex}(\omega, A)/\partial\omega]_{\omega=\omega_0, A=A_0}$ and

$$\eta_{21} = \frac{P_o}{P_e} = \frac{R_L}{R_0}\left|\frac{-R_0 + j\overline{X}(A_0) + Z_{11}(\omega_0)}{R_L + Z_{22}(\omega_0)}\right| \quad \text{(B2)}$$

where $P_e = R_0 A_0^2/2$ is the power generated by the active device and P_o is the output power dissipated in R_L. For later use, other relations corresponding to (A6) and (A9) are given:

$$Z_{12}^2(\omega_0) = [-R_0 + j\overline{X}(A_0) + Z_{11}(\omega_0)][R_L + Z_{22}(\omega_0)] \quad \text{(B3)}$$

$$Z'(\omega_0)/Z_{ex}'(\omega_0) = [-R_0 + j\overline{X}(A_0) + Z_{11}(\omega_0)]/[R_L + Z_{22}(\omega_0)]. \quad \text{(B4)}$$

We now define the loaded Q and external Q of the oscillator circuit by

$$Q_{L,c} = \omega_0 |Z'(\omega_0)|/2R_0 \quad \text{(B5)}$$

$$Q_{ex,c} = \omega_0 |Z_{ex}'(\omega_0)|/2R_L. \quad \text{(B6)}$$

Then from (B1) we have

$$Q_{L,c}/Q_{ex,c} = \eta_{21} \quad \text{(B7)}$$

which is usually termed the circuit efficiency of the oscillator.

If matched load R_L and the port 2-2' in Fig. 1(a) are connected via a transmission line, it can easily be shown that $|Z_{ex}'(\omega_0)|$ or $Q_{ex,c}$ is invariant under the shift of the reference plane of port 2-2'. $Z_{ex}'(\omega_0)$ becomes purely imaginary at a new reference plane shifted from the original position by $(\lambda_g/4\pi)[\tan^{-1}[1/\arg\{Z_{ex}'(\omega_0)\}] + n\pi]$, where n is an integer. At one of these new reference planes, $X_{ex}' \equiv \text{Im}\{Z_{ex}'(\omega_0)\}$ is positive and $Q_{ex,c}$ is given by

$$Q_{ex,c} = \omega_0 X_{ex}'(\omega_0)/2R_L.$$

This is just the usual definition of Q_{ex} in microwave circuits [20]. It is also to be noted that $Q_{ex,c}$ or $Q_{L,c}$ may not always be equivalent to the physically defined Q, i.e., $\omega_0\times$(total stored energy)/(power dissipation), in the case of multiple-resonant circuits.

Meanwhile, the conventional Q_{ex} of an oscillator is measured from injection-locking and frequency-pulling experiments. It will be shown later that such a Q_{ex} is

related to $Q_{ex,c}$ as

$$Q_{ex} = Q_{ex,c} \sin(\Theta - \theta) = \frac{\omega_0 |Z_{ex}'(\omega_0)|}{2R_L} \sin(\Theta - \theta). \quad \text{(B8)}$$

By analogy, we also define Q_L of the oscillator by

$$Q_L = Q_{L,c} \sin(\Theta - \theta) = \frac{\omega_0 |Z'(\omega_0)|}{2R_0} \sin(\Theta - \theta) \quad \text{(B9)}$$

where $Q_L/Q_{ex} = \eta_{21}$. Thus we had better distinguish Q of an oscillator from that of an oscillator circuit.

C. Q_{ex} in Injection-Locking Experiments

Usually, Q_{ex} of an oscillator is experimentally found by the locking equation:

$$\frac{\Delta f}{f_0} = \frac{2}{Q_{ex}} \sqrt{\frac{P_i}{P_o}} \quad \text{(C1)}$$

where Δf is the total locking range, P_o is the free-running output power, and P_i is the injected signal power. It will be shown that such a Q_{ex} is represented by (B8). According to Kurokawa [8], the locking range is determined by

$$A_0 |rAR - sAX| / a_0(s^2 + r^2)^{1/2} \leqq 1. \quad \text{(C2)}$$

If $|\omega_i - \omega_0|$ is small we have

$$AR \equiv R(\omega_i) - R(\omega_0) \fallingdotseq R'(\omega_0)(\omega_i - \omega_0)$$
$$AX \equiv X(\omega_i) - X(\omega_0) \fallingdotseq X'(\omega_0)(\omega_i - \omega_0)$$

where ω_i is the angular frequency of the injected signal. From these and from (11) in the text, the inequality (C2) becomes

$$\frac{A_0}{a_0} |Z'(\omega_0)| |\omega_i - \omega_0| \sin(\Theta - \theta) \leqq 1. \quad \text{(C3)}$$

Since A_0 is the amplitude of the current through the device and a_0 is the equivalent voltage of the injected signal in series with the device, they are given by

$$A_0 = (2P_c/R_0)^{1/2} = (2P_o/R_0\eta_{21})^{1/2}$$
$$a_0 = \left|\frac{Z_{12}(\omega_i)}{R_L + Z_{22}(\omega_i)}\right| (8R_L P_i)^{1/2} \fallingdotseq \left|\frac{Z_{12}(\omega_0)}{R_L + Z_{22}(\omega_0)}\right| (8R_L P_i)^{1/2}$$
$$= (8R_0\eta_{21}P_i)^{1/2}.$$

Substituting these into (C3) we have a locking equation:

$$\frac{\Delta\omega}{\omega_0} = \frac{4R_0\eta_{21}}{\omega_0 |Z'(\omega_0)| \sin\{\Theta - \theta\}} \sqrt{\frac{P_i}{P_o}}$$
$$= \frac{4R_L}{\omega_0 |Z_{ex}'(\omega_0)| \sin(\Theta - \theta)} \sqrt{\frac{P_i}{P_o}}.$$

Comparison between the above equation and (C1) shows that the Q_{ex} is represented by (B8).

D. Q_{ex} in Frequency-Pulling Experiments

Another conventional method to evaluate Q_{ex} of an oscillator is the frequency pulling. Such a Q_{ex} is also represented by (B8), as shown below. Presume load Z_L, which has a reflection coefficient $\Gamma = \alpha e^{j\phi}$ ($0 \leqq \phi \leqq 2\pi$, where $\alpha \ll 1$), is connected to port 2-2' of Fig. 1(a) instead of a matched load R_L. Then the condition of oscillation becomes

$$Z_{ex}(\omega, A) + Z_L = 0 \quad \text{(D1)}$$

where

$$Z_L = R_L \frac{1 + \Gamma}{1 - \Gamma} \fallingdotseq R_L(1 + 2\alpha e^{j\phi}).$$

If $|\omega - \omega_0|$ and $|A - A_0|$ is small, Z_{ex} is expanded as

$$Z_{ex}(\omega, A) = Z_{ex}(\omega_0, A_0) + Z_{ex}'(\omega_0)(\omega - \omega_0) + \dot{Z}_{ex}(A_0)(A - A_0)$$

where $Z_{ex}'(\omega_0) \equiv [\partial Z_{ex}(\omega, A)/\partial\omega]_{\omega=\omega_0, A=A_0}$, $Z_{ex}(\omega_0, A_0) = -R_L$, and

$$\dot{Z}_{ex}(A_0) \equiv [\partial Z_{ex}(\omega, A)/\partial A]_{\omega=\omega_0, A=A_0} = \frac{Z_{12}^2(\omega_0)\left[-\frac{d\overline{R}}{dA} + j\frac{d\overline{X}}{dA}\right]}{[-\overline{R}(A_0) + j\overline{X}(A_0) + Z_{11}(\omega_0)]^2}.$$

Employing (B2)~(B4) we have

$$\dot{Z}_{ex}(A_0) = \frac{R_0(s + jr)}{A_0} \frac{Z_{ex}'(\omega_0)}{Z'(\omega_0)} = \frac{R_L}{A_0\eta_{21}} \sqrt{s^2 + r^2}\, e^{j(\theta - \Theta + \psi)}$$

where $s + jr = \sqrt{s^2 + r^2} e^{j\theta}$, $Z'(\omega_0) = |Z'(\omega_0)| e^{j\Theta}$, and $Z_{ex}'(\omega_0) = |Z_{ex}'(\omega_0)| e^{j\psi}$.

Hence, (D1) becomes

$$|Z_{ex}'(\omega_0)| (\omega - \omega_0) e^{j\psi} + \frac{R_L}{\eta_{21}} \sqrt{s^2 + r^2} \frac{A - A_0}{A_0} e^{j(\theta + \psi - \Theta)} + 2\alpha R_L e^{j\phi} = 0.$$

From this, we obtain

$$\omega - \omega_0 = \frac{2\alpha R_L \sin(\theta - \Theta + \psi - \phi)}{|Z_{ex}'(\omega_0)| \sin(\Theta - \theta)}.$$

By varying ϕ from 0 to 2π, the total frequency shift $\Delta\omega$ is given by

$$\frac{\Delta\omega}{\omega_0} = \frac{4\alpha R_L}{\omega_0 |Z_{ex}'(\omega_0)| \sin(\Theta - \theta)}.$$

On the other hand, we conventionally evaluate Q_{ex} from the measured $\Delta\omega$ by

$$Q_{ex} = \frac{2\omega_0}{\Delta\omega} |\Gamma| = \frac{2\alpha\omega_0}{\Delta\omega}.$$

Hence, we have again (B8).

ACKNOWLEDGMENT

The author wishes to thank Y. Sawayama for many helpful discussions and suggestions, M. Morita for his assistance in noise measurements, I. Kuru and K. Hirai for supplying Gunn diodes and oscillators, and S. Okano and M. Kashiwagi for supplying Si and GaAs avalanche diodes.

REFERENCES

[1] J. Josenhans, "Noise spectra of Read diode and Gunn oscillators," *Proc. IEEE* (Lett.), vol. 54, pp. 1478–1479, Oct. 1966.
[2] J. G. Ondria and J. C. Collinet, "Investigation of noise reduction techniques of solid-state type microwave sources," in *1968 Int. Solid-State Circuits Conf., Dig. Tech. Papers*, pp. 82–83.
[3] E. F. Scherer, "Investigations of the noise spectra of avalanche oscillators," *IEEE Trans. Microwave Theory Tech.* (*Special Issue on Noise*), vol. MTT-16, pp. 781–788, Sept. 1968.
[4] J. R. Ashley and F. M. Palka, "Noise properties and stabilization of Gunn and avalanche diode oscillators and amplifiers," in *1970 G-MTT Int. Microwave Symp. Dig.*, pp. 161–164.
[5] ——, "Reduction of FM noise in microwave diode oscillators by cavity and injection stabilization," in *1971 G-MTT Int. Microwave Symp. Dig.*, pp. 94–95.
[6] W. A. Edson, "Noise in oscillators," *Proc. IRE*, vol. 48, pp. 1454–1466, Aug. 1960.
[7] J. A. Mullen, "Background noise in nonlinear oscillators," *Proc. IRE*, vol. 48, pp. 1467–1473, Aug. 1960.
[8] K. Kurokawa, "Noise in synchronized oscillators," *IEEE Trans. Microwave Theory Tech.*, vol. MTT-16, pp. 234–240, Apr. 1968.
[9] ——, "Some basic characteristics of broadband negative resistance oscillator circuits," *Bell Syst. Tech. J.*, vol. 48, pp. 1937–1955, July–Aug. 1969.
[10] Y. Okabe and S. Okamura, "Analysis of stability and noise of oscillators in free-running, synchronized-running and parallel-running," *J. Inst. Electron. Commun. Eng. Jap.*, vol. 12, pp. 755–762, Dec. 1969.
[11] W. B. Davenport and W. L. Root, *Randon Signals and Noise.* New York: McGraw-Hill, 1958, ch. 6.
[12] L. S. Cutler and C. L. Searle, "Some aspects of the theory and measurement of frequency fluctuations in frequency standards," *Proc. IEEE* (*Special Issue on Frequency Stability*), vol. 54, pp. 136–154, Feb. 1966.
[13] M. E. Hines, "Potential applications and the noise problem in the Read avalanche diode," in *1966 Int. Solid-State Circuits Conf., Dig. Tech. Papers*, pp. 82–83.
[14] M. Ohtomo and Y. Sawayama, "Noise measurement of microwave solid-state oscillators," in *1971 Nat. Conf. Rec. Inst. Electron. Commun. Eng. Jap.*, no. 568.
[15] J. R. Ashley, C. B. Searles, and F. M. Palka, "The measurement of oscillator noise at microwave frequencies," *IEEE Trans. Microwave Theory Tech.* (*Special Issue on Noise*), vol. MTT-16, pp. 753–760, Sept. 1968.
[16] J. G. Ondria, "A microwave system for measurements of AM and FM noise spectra," *IEEE Trans. Microwave Theory Tech.* (*Special Issue on Noise*), vol. MTT-16, pp. 767–781, Sept. 1968.
[17] A. A. Sweet and L. A. MacKenzie, "The FM noise of a CW Gunn oscillator," *Proc. IEEE* (*Special Issue on Detection Theory and Its Applications*) (Lett.), vol. 58, pp. 822–823, May 1970.
[18] E. F. Scherer, "Circuit techniques for the noise reduction and frequency stabilization of avalanche diode oscillators," in *1968 G-MTT Int. Microwave Symp. Dig.*, pp. 63–71.
[19] M. Kashiwagi, S. Okano, T. Utagawa, and M. Takabayashi, "GaAs IMPATT diode," in *1970 Joint Conv. Rec. Four Inst. Electron. Eng. Jap.*, no. 1743.
M. Kashiwagi, T. Utagawa, S. Okano, and M. Ohtomo, "*X*-band GaAs IMPATT diode," *Inst. Electron. Commun. Eng. Jap.*, Nov. 1970, ED 70-31.
[20] D. L. Scharfetter and H. K. Gummel, "Large-signal analysis of a silicon Read diode oscillator," *IEEE Trans. Electron Devices*, vol. ED-16, pp. 64–77, Jan. 1969.
[21] M. Ohtomo, "Reflection-type IMPATT diode power amplifier for 11-GHz band," *Inst. Electron. Commun. Eng. Jap.*, July 1970, ED 70-14.
[22] C. G. Montgomery, R. H. Dicke, and E. M. Purcell, *Principles of Microwave Circuits*, M.I.T. Rad. Lab. Series 8. New York: McGraw-Hill, 1948, ch. 4, 5, and 7.

First-Order Nonlinear Theory in Hexagonal Ferrites with Planar Anisotropy under Perpendicular Pumping

JOSEPH HELSZAJN, MEMBER, IEEE, AND JOHN MCSTAY

***Abstract*—The first-order spinwave instability under perpendicular pumping at large signal power in an hexagonal ferrite ellipsoid with planar anisotropy biased in the easy plane is studied. The nonlinear coupling coefficient is obtained in terms of the physical variables of the unstable spinwaves and the uniform mode magnetization such as the orientation and ellipticity of the unstable spinwaves, the coordinates of the spinwave propagation vector k, and the uniform mode ellipticity. Results obtained using a computer in the case of a sphere are included. Also included are experimental results on the coincidence region with the dc field in the easy plane and with the dc field out of the easy plane. This latter arrangement leads to a new tunable coincidence limiter.**

Manuscript received February 5, 1970; revised August 19, 1970. This work was supported by the Ministry of Technology, England.

J. Helszajn is a consultant, 3 Abercromby Place, Edinburgh 3, Scotland.
J. McStay is with the Department of Electronic Engineering, the University of Leeds, Leeds, England.

I. INTRODUCTION

THE first- and second-order nonlinear behavior in isotropic ferrites under perpendicular pumping at large signal power due to spinwave instabilities are well known [1]–[5]. The first-order nonlinear process is usually the more important one and is the only one considered in this paper. This instability gives rise to an additional subsidiary resonance peak below the mag-